Acta Astronautica 102 (2014) 67–80

Contents lists available at ScienceDirect

Acta Astronautica

journal homepage: www.elsevier.com/locate/actaastro

Development and hardware-in-the-loop test of a guidance, navigation and control system for on-orbit servicing

Heike Benninghoff*, Florian Rems, Toralf Boge

German Aerospace Center (DLR), 82234 Wessling, Germany

ARTICLE INFO

Article history:
Received 13 January 2014
Received in revised form
15 April 2014
Accepted 19 May 2014
Available online 29 May 2014

Keywords:
Orbital servicing
Ground-based rendezvous
Hardware-in-the-loop
Simulation
Navigation with delayed measurements
Telepresence

ABSTRACT

The rendezvous phase is one of the most important phases in future orbital servicing missions. To ensure a safe approach to a non-cooperative target satellite, a guidance, navigation and control system which uses measurements from optical sensors like cameras was designed and developed. During ground-based rendezvous, stability problems induced by delayed position measurements can be compensated by using a specially adapted navigation filter. Within the VIBANASS (VIsion BAsed NAvigation Sensor System) test campaign, hardware-in-the-loop tests on the terrestrial, robotic based facility EPOS 2.0 were performed to test and verify the developed guidance, navigation and control algorithms using real sensor measurements. We could demonstrate several safe rendezvous test cases in a closed loop mode integrating the VIBANASS camera system and the developed guidance, navigation and control system to a dynamic rendezvous simulation.

1. Introduction

Technology for on-orbit servicing is developed and missions demonstrating orbital servicing capabilities are currently in preparation [1–4]. Applications of on-orbit servicing are life time extension of partly damaged satellites and de-orbiting of in-operative satellites at the end of their life [5]. The rendezvous phase is one of the most critical parts of a robotic servicing mission since a safe approach to a non-cooperative target satellite must be conducted.

To approach a target satellite, optical sensors such as mono and stereo cameras can be used for relative navigation. Raw camera data is processed to provide a measurement of the relative position between the two spacecrafts. Alternatively, an operator on ground can be involved who marks the position of the target satellite in camera images and thus supports or replaces the automatic object recognition.

Rendezvous and docking via teleoperation can be done in the framework of a geostationary robotic serving mission like OLEV [3] and within a low Earth orbit mission using a data relay satellite [2]. A critical problem arising from the teleoperation concept is time delay. The delay can cause stability problems if the guidance, navigation and control (GNC) system is not specially developed to handle measurements with delay. Stability problems are very critical if high dynamics are involved. For example, during the ROKVISS experiment [6], where modern telerobotic technology was demonstrated, special control methods were applied to compensate for time delays. Using standard communication architecture, time delays of 2–5 s are expected for future geostationary on-orbit servicing [3] and even up to 10 s are expected in the ConeXPress-OLEV study [7]. About 7 s of delay (round-trip delay) was faced

* Corresponding author.
E-mail addresses: Heike.Benninghoff@dlr.de (H. Benninghoff), Florian.Rems@dlr.de (F. Rems), Toralf.Boge@dlr.de (T. Boge).

http://dx.doi.org/10.1016/j.actaastro.2014.05.023
0094-5765/

during the ETS-VII mission (Japanese Engineering Test Satellite VII) where a bilateral teleoperation experiment via a data relay satellite was performed [8].

Before an on-orbit servicing mission can be launched, intensive test, verification and validation of the rendezvous sensors and of the GNC system are necessary. Hardware-in-the-loop (HiL) simulations are suitable to test real hardware like cameras in an almost realistic scenario including simulation of illumination conditions and of the satellites' relative motion [9–11]. In a closed loop rendezvous simulation the full control loop can be tested consisting of sensor, processing unit, guidance, navigation, control and simulation of actuators and the spacecrafts' dynamical relative motion.

There are several approaches for rendezvous to a non-cooperative satellite in space. In [12], the authors cope with the problem of recognizing an uncooperative target satellite. Pose estimation methods for rendezvous and docking applications are proposed in [13]. A GNC system for rendezvous is presented in [14]. First demonstrations of ground-based rendezvous were already performed in the extended phase of the PRISMA mission. The German Aerospace Center demonstrated a controlled approach from 30 km to 3 km in the ARGON (Advanced Rendezvous demonstration using GPS and Optical Navigation) experiment [15].

Different ground facilities exist for testing GNC algorithms and simulating rendezvous and docking maneuvers. In the framework of an Italian project called STEPS (Systems and Technologies for Space Exploration) a Rendezvous and Docking simulator based on an air-floating test bed (2D platform) and GNC algorithms are developed [16]. Hardware-in-the-loop tests of a 3D LIDAR (Light Detection and Ranging) executed at the Spacecraft Robotics Engineering and Controls Lab of the U.S. Naval Research Laboratory are described in [17]. The authors observed also time delays induced by the sensor hardware and by data interfaces. The European Proximity Operations Simulator (EPOS) 2.0 [18,9] is a robotic based test bed allowing for rendezvous and docking simulation and sensor and GNC system verification. Several hardware-in-the-loop tests without simulating time delay have been conducted [11]. EPOS 2.0 was also involved as test facility in the VIBANASS project (VIsion BAsed NAvigation Sensor System). In this project an optical rendezvous and docking camera system was developed [19] and tests and verification of the camera system were conducted at the simulator EPOS 2.0 in an open loop mode for verification of the sensor system and the image processing module [20,21]. An overview of ground verification methods and facilities is given in the survey article [22].

Development of a GNC system which can handle delayed measurements and test of the entire control loop during an approach under realistic conditions are still open research tasks. In particular, a safe approach has to be tested and demonstrated using real sensor data within a hardware-in-the loop simulation. The stability of the control loop in the case of delayed measurements has to be proved. In the final VIBANASS test campaign, a secondary goal was to demonstrate closed loop rendezvous simulation with the VIBANASS camera system. Existing approaches [11] using Kalman filter techniques had to be consequently modified for this task.

The objective of this paper is to present a hardware-in-the-loop simulation for testing closed loop rendezvous processes within the VIBANASS test campaign at EPOS. The main task is to develop a guidance, navigation and control system resulting in a stable control loop even in the case of delayed position measurements.

Throughout the paper, a *closed loop simulation* is a simulation in which the output of a GNC system is fed back to the simulation of the actuators and spacecrafts' dynamics. Thus, the trajectory of an approach is not predefined but computed in real-time. The trajectory depends on the sensor measurements, the guidance values and the design of the navigation filter and of the controller. *Time delay* is the time difference between the capturing of the images by a camera and the time when the measurements are available for the navigation system. The active satellite in an on-orbit servicing mission is called *servicer* or *chaser*; the passive satellite is called *client* or *target*.

2. Methods

2.1. Hardware-in-the-loop simulator EPOS 2.0

EPOS, the European Proximity Operations Simulator, is a hardware-in-the-loop simulator focusing on the last phase (25–0 m) of Rendezvous and Docking (RvD) maneuvers involving two spacecraft. The simulation concept of EPOS takes advantage of both physical and computer simulation: on one hand, satellite dynamics cannot be simulated physically on ground for any practical purposes, while numerical simulation can be realized easily and leads to very good results. On the other hand, realistic sensor output including various physical effects is very difficult to simulate with sufficient quality by pure numeric software. EPOS allows for the combination of numerical satellite dynamics simulation and real RvD sensor hardware.

Fig. 1 illustrates the facility layout. The central elements constitute two standard industrial robots. Robot 1 in Fig. 1 is a KUKA KR100HA, which can carry a maximum payload of 100 kg. It is mounted on a linear rail with a length of 25 m. The robot can be moved on that rail in order to simulate the relative distance of two satellites in space. The other robot (robot 2) is a KUKA KR240. Its maximum payload is 240 kg. In contrast to robot 1, it is mounted at the end of the rail, its base fixed in the laboratory. Each robot is equipped with a breadboard attached to the tool flange which can be used to mount satellite mockups or sensor devices.

If visual RvD sensors are involved, realistic reproduction of light with a Sun-like irradiation intensity and a spectrum is crucial. For example, during VIBANASS open-loop tests (cf. Section 2.2) realistic illumination conditions including different incident angles had to be realized. For that purpose, a spotlight with a spectrum very close to the Sun is used at EPOS [10].

2.2. VIBANASS test campaign on EPOS

In the VIBANASS project an optical rendezvous and docking camera system was developed [19,21,23]. The

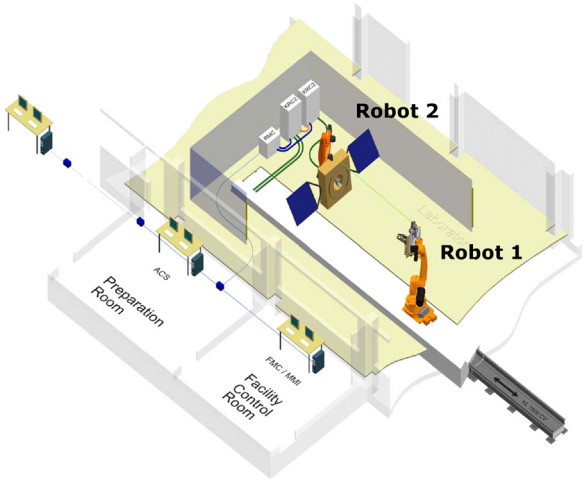

Fig. 1. Layout of EPOS facility – two industrial robots simulating the last 25 m of the rendezvous phase and a PC based monitoring and control system.

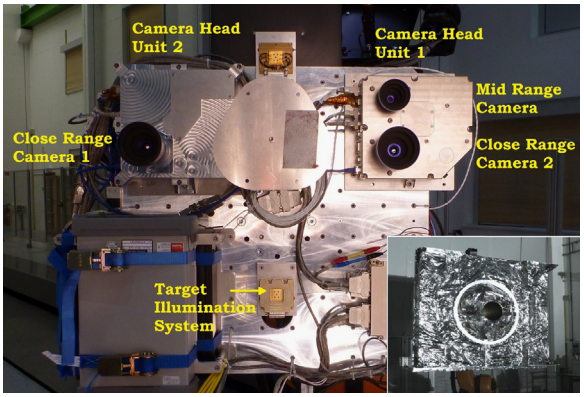

Fig. 2. Test setup: VIBANASS sensor system with mid and close range camera and image of the client mockup.

requirements were based on low Earth orbit and geostationary on-orbit servicing scenarios like DEOS (DEutsche Orbitale Servicing Mission – German Orbital Servicing Mission) and OLEV (Orbital Life Extension Vehicle).

VIBANASS consists of three cameras using different optics intended for far, mid and close range rendezvous. All three sensors are based on the same CMOS chip which captures 10 bit gray scale images with a resolution of 1024×1024 pixels. The camera system further comprises all necessary control and power supply hardware and image processing software like JPEG compression and optical correction. The VIBANASS system can be configured for mono and stereo image acquisition. Stereo images are mainly used for close range rendezvous. VIBANASS further contains a laser-based target illumination system which improves the quality of images captured by the close range camera. A detailed technical description of the camera and of the target illumination system is given in [19]. An image processing system [24] is used for VIBANASS which continuously tracks the target from camera images and which computes an estimation of the 3D relative position of the target with respect to the camera.

Tests and verification of the mid and close range cameras were conducted at EPOS 2.0 [21,23]. The VIBANASS demonstrator model contained a camera system with a close range stereo camera, a mid range mono camera and a target illumination system. The sun simulator of the EPOS facility was used to simulate different incident angles and thus different illumination conditions. The robot on the linear slide carried the VIBANASS sensor system and acted as a service satellite, whereas the second robot carried a mock-up of a typical geostationary satellite, see Fig. 2.

In the VIBANASS test campaign, open-loop tests were performed where the camera system and the image processing system were tested and verified under different illumination conditions (incident angle of the Sun simulator, brightness of the light), different trajectories and different camera settings (e.g. different image compression). GPS time was used for time synchronization between the sensor system and the EPOS facility such that the images could be off-line post-processed using the EPOS log data as reference data.

A more realistic rendezvous simulation was additionally conducted by embedding the camera and the image processing system in a closed loop simulation. In the framework of the closed-loop rendezvous simulation, the robots did not move according to a predefined trajectory but represented as a realistic movement of two satellites in space based on physical equations of motions. Sensor data was processed by the image processing unit and the navigation system and handled over to the controller. The controller output was fed back to the actuator and the satellite simulator. GPS time was used again to provide a time stamp for each captured image; a necessary information to compensate for time delays, see Section 2.3.2.

An existing closed loop rendezvous simulation concept [11] was adapted and modified for the VIBANASS setup. The main challenge was the handling of measurements with delay which can occur during on-orbit servicing with teleoperation.

Fig. 3 shows a ground-based rendezvous and docking scenario involving geostationary satellites (left) and the simulation concept at EPOS for closed loop hardware-in-the-loop rendezvous tests (right). In a ground-based on-orbit servicing mission, images of the rendezvous cameras are provided via telemetry to the ground. The image processing, which provides relative position measurements, and the corresponding guidance, navigation and control algorithms are computed on ground and are supervised by an operator. The resulting telecommands e.g. the actuators of the servicer or commands for the sensor control are sent to the satellite. At EPOS, the space segment is simulated by the manipulators which are controlled in real-time. Their motion is computed by a dynamical satellite simulator. Furthermore, interfaces to the cameras are established for control of the sensors and acquisition of image data. The payload control system contains the image processing system and the GNC system for the control of the relative position.

2.3. Numerical simulator

The numerical simulator contains all elements which are not represented by real hardware. These comprise dynamical and kinematical models for the position and orientation of the

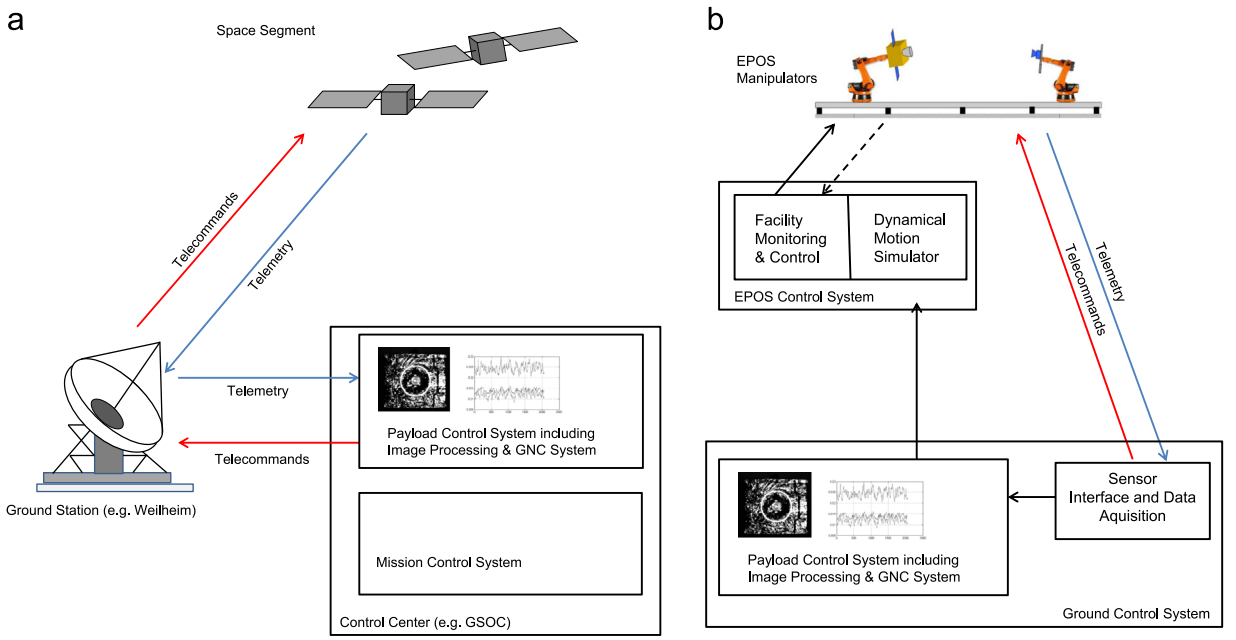

Fig. 3. Left: rendezvous and docking scenario with teleoperation including space segment, ground station and control center, right: simulation concept for rendezvous and docking via teleoperation at EPOS.

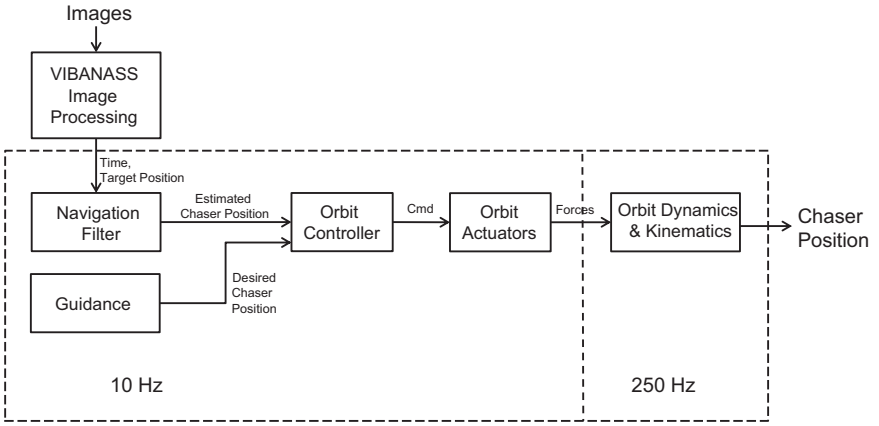

Fig. 4. Chaser spacecraft simulator for VIBANASS.

target and the chaser spacecraft, actuator models and the guidance, navigation and control system. Further, those sensors which are not available as real hardware in the VIBANASS setup have to be simulated and are part of the numerical simulator.

Fig. 4 gives an overview on the numerical simulator for the chaser spacecraft. The images captured by the VIBANASS camera system are processed by the image processing unit, see [24] for a detailed description of the target tracking algorithm. The input to the navigation system is the measured target position with respect to the camera and the time of the image capturing. Based on the position measurements, a navigation filter determines an estimation of the chaser's relative position with respect to the target. A guidance system delivers the desired position of the chaser. The orbit controller compares the estimated relative chaser position with the desired relative position and computes the necessary commands for the actuators.

Actuator models transform the commands to forces. These are passed to the orbit dynamics and kinematics models which realize equations of motion for the orbit of the chaser. The solution of the equations, i.e. the chaser's position, is commanded in real-time to the EPOS facility. Similarly, equations of motion for the target's position are solved and commands are sent to the facility.

The EPOS manipulators move according to the commanded values and thus stimulate the VIBANASS camera sensor system. The EPOS testbed requires a commanding rate of 250 Hz. Therefore the orbit dynamics and kinematics are executed every 4 ms, whereas the GNC system and the actuator models run every 100 ms.

Among the systems visualized by Fig. 4, the guidance, the image processing, the navigation filter and the orbit controller are executed on-ground (cf. Fig. 3).

The attitude control system is part of the space segment and thus not affected by any delay. At EPOS, the dynamical motion simulator (cf. Fig. 3, right sub-figure) has to generate both position and attitude commands for the 6 DOF manipulators. Therefore, a simple attitude system is realized in the numerical simulator. The attitude dynamics and kinematics are based on the Euler equation and the quaternion differential equation, cf. [25].

The following sections describe the single elements of the closed loop rendezvous simulation in detail.

2.3.1. Orbit dynamics and kinematics

The objective is to develop a realistic simulation of the rendezvous process including the real orbit mechanics. A numerical model based on equations of motion is implemented to emulate the realistic motion of the two satellites in orbit. The position and the velocity are described in the Clohessy Wiltshire (CLW) coordinate framework, see [26]. It is a local coordinate system whose origin is aligned with the center of mass of the target spacecraft. Thus, the chaser's position is described in the local orbital frame of the target. Table 1 explains the axes of the CLW coordinate system.

The Hill equations describe the relative motion of the active or service spacecraft with respect to the target spacecraft on a circular orbit with orbit rate ω_0. The Hill equations are a system of linear, ordinary differential equations for the position $\vec{p}=(p_x,p_y,p_z)$ and the velocity $\vec{v}=(\dot{p}_x,\dot{p}_y,\dot{p}_z)=(v_x,v_y,v_z)$ of the service satellite in the CLW framework, cf. [26]:

$$\ddot{p}_x = 2\omega_0\dot{p}_z+\frac{1}{m}f_x, \tag{1a}$$

$$\ddot{p}_y = -\omega_0^2 p_y+\frac{1}{m}f_y, \tag{1b}$$

$$\ddot{p}_z = -2\omega_0\dot{p}_x+3\omega_0^2 p_z+\frac{1}{m}f_z. \tag{1c}$$

Here, m is the mass of the satellite, $\vec{f}=(f_x,f_y,f_z)$ is the sum of external forces acting on the satellite, $\dot{u}$ denotes the derivative with respect to time of a time-dependent function u, $\ddot{u}$ ia the second time-derivative of u.

Given the initial conditions, i.e. position and velocity at time $t=0$, the initial value problem can be solved with standard numerical methods like Runge–Kutta methods. In practice, for simulation on EPOS we use the simple explicit Euler scheme as a numerical solver since this is prescribed by the real-time configuration at EPOS.

2.3.2. Navigation filter with delay

The navigation filter gives an estimate of the relative position and a velocity of the service satellite with respect to the target based on prior knowledge of the state combined with measurements observed over time.

We first consider a discrete, linear system with non-delayed measurements and additive Gaussian noise

$$\vec{x}_{k+1} = F_k\vec{x}_k+G_k\vec{u}_k+\vec{v}_k, \quad \vec{v}_k\sim N(0,Q_k), \tag{2a}$$

$$\vec{z}_k = H_k\vec{x}_k+\vec{\omega}_k, \quad \vec{\omega}_k\sim N(0,R_k), \tag{2b}$$

where $\vec{x}_k\in\mathbb{R}^n$ denotes the state vector, $\vec{u}_k\in\mathbb{R}^l$ the input or control vector, $\vec{v}_k\in\mathbb{R}^n$ the system noise with zero mean and covariance $Q_k\in\mathbb{R}^{n\times n}$, $\vec{z}_k\in\mathbb{R}^m$ denotes the measurement and $\vec{\omega}_k\in\mathbb{R}^m$ the measurement noise with zero mean and covariance $R_k\in\mathbb{R}^{m\times m}$. Further $F_k\in\mathbb{R}^{n\times n}$, $G_k\in\mathbb{R}^{n\times l}$, $H_k\in\mathbb{R}^{m\times n}$ are matrices describing the linear relation between $\vec{x}_{k+1}$ and $\vec{x}_k$ and $\vec{u}_k$ as well as the linear relation between $\vec{z}_k$ and $\vec{x}_k$.

The Kalman filter [27] algorithm states a recursive solution to the filtering problem (2). It consists of predictor and corrector steps to determine an estimation $\vec{x}^{\,\mathrm{est}}_k$ of the state and an estimation P^{est}_k of the covariance of $\vec{x}_k-\vec{x}^{\,\mathrm{est}}_k$. The algorithm is given by

$$\vec{x}^{\,\mathrm{pre}}_{k+1} = F_k\vec{x}^{\,\mathrm{est}}_k+G_k\vec{u}_k, \tag{3a}$$

$$P^{\mathrm{pre}}_{k+1} = F_kP^{\mathrm{est}}_kF_k^T+Q_k, \tag{3b}$$

$$K_{k+1} = P^{\mathrm{pre}}_{k+1}H_{k+1}^T(H_{k+1}P^{\mathrm{pre}}_{k+1}H_{k+1}^T+R_{k+1})^{-1}, \tag{3c}$$

$$\vec{x}^{\,\mathrm{est}}_{k+1} = \vec{x}^{\,\mathrm{pre}}_{k+1}+K_{k+1}(\vec{z}_{k+1}-H_{k+1}\vec{x}^{\,\mathrm{pre}}_{k+1}), \tag{3d}$$

$$P^{\mathrm{est}}_{k+1} = (1-K_{k+1}H_{k+1})P^{\mathrm{pre}}_{k+1}, \tag{3e}$$

see [27,28] for reference.

Now, we consider a measurement $\vec{z}^{\,D}_k$ which is delayed by N samples. The corresponding measurement equation can be formulated as

$$\vec{z}^{\,D}_k = H_s\vec{x}_s+\vec{\omega}_s, \quad s:=k-N. \tag{4}$$

Thus, $\vec{z}^{\,D}_k$ is the measurement of the state $\vec{x}_s$ at time t_s, $s=k-N$. For the filter, the measurement is available at time t_k.

More generally, the time when the measurements are performed need not be synchronized with the discrete time steps when the filter is executed. We therefore consider

$$\vec{z}^{\,D}_k = \vec{z}(t)=H(t)\vec{x}(t)+\vec{\omega}(t), \tag{5}$$

where $t\le t_k$. The delayed filter problem is illustrated in Fig. 5.

At time t_k, we face the following delay problem: the measurement $\vec{z}_k=\vec{z}(t_k)$ is not available yet. The most recent available measurement is $\vec{z}(t)$, $t<t_k$. A simple and intuitive way of adapting the Kalman filter algorithm for

Table 1
Clohessy Wiltshire coordinate framework.

Axis	Axis name	Description
x	V-Bar	Tangential direction, i.e. direction of the orbital velocity vector
y	H-Bar	Opposite direction of the angular momentum vector of the orbit, i.e. parallel to the normal vector of the orbit plane
z	R-Bar	Direction to Earth, i.e. radial from the spacecraft's center of mass to the center of the Earth

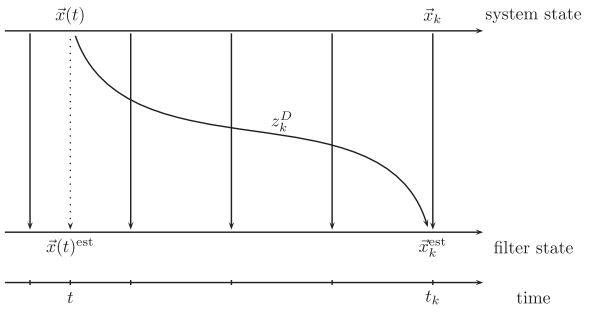

Fig. 5. Delayed filter problem.

delayed measurements is to replace the measurement residuum $\vec{z}_{k+1} - H_{k+1}\vec{x}_{k+1}^{\text{pre}}$ in (3d) by

$$\Delta\vec{z}_k^D := \vec{z}(t) - H(t)\vec{x}(t)^{\text{est}}, \tag{6}$$

where $\vec{x}(t)^{\text{est}}$ is an estimation of the state at time t. Therefore, let $t \in [t_{s-1}, t_s]$, for some $s \le k$. We interpolate to get an estimation of the state at time t:

$$\vec{x}(t)^{\text{est}} := \frac{t_s - t}{t_s - t_{s-1}}\vec{x}_{s-1}^{\text{est}} + \frac{t - t_{s-1}}{t_s - t_{s-1}}\vec{x}_s^{\text{est}}. \tag{7}$$

The update equation (3d) is slightly changed to

$$\vec{x}_{k+1}^{\text{est}} = \vec{x}_{k+1}^{\text{pre}} + K_{k+1}\Delta\vec{z}_{k+1}^D. \tag{8}$$

The setting of the measurement residuum (6) can be mathematically justified by the following considerations which are based on linear extrapolation and first order Taylor series approximation: the basic idea is to extrapolate the measurement by setting

$$\vec{z}_k^{\text{extra}} := \vec{z}(t) + H_k\vec{x}_k^{\text{pre}} - H(t)\vec{x}(t)^{\text{est}}. \tag{9}$$

Eq. (9) can be motivated by considering the measurement equation and a Taylor series expansion of $\vec{\omega}(t+\Delta t)$ around t with $\Delta t := t_k - t > 0$:

$$\begin{aligned}\vec{z}(t+\Delta t) &= H(t+\Delta t)\vec{x}(t+\Delta t) + \vec{\omega}(t+\Delta t)\\ &= H(t+\Delta t)\vec{x}(t+\Delta t) + \vec{\omega}(t)\\ &\quad + \Delta t\dot{\vec{\omega}}(t) + \mathcal{O}(\Delta t^2)\\ &= \vec{z}(t) + H(t+\Delta t)\vec{x}(t+\Delta t) - H(t)\vec{x}(t)\\ &\quad + \Delta t\dot{\vec{\omega}}(t) + \mathcal{O}(\Delta t^2).\end{aligned} \tag{10}$$

The state $\vec{x}(t)$ at time t is replaced by the estimation $\vec{x}(t)^{\text{est}}$ defined in (7). The state $\vec{x}(t+\Delta t)$ at time $t+\Delta t = t_k$ is replaced by the best available estimation $\vec{x}_k^{\text{pre}}$. The terms $\Delta t\dot{\vec{\omega}}(t) + \mathcal{O}(\Delta t^2)$ are omitted in the estimation. Therefore, the expression (10) is approximated by (9).

The measurement residuum is defined as

$$\Delta\vec{z}_k^D = \vec{z}_k^{\text{extra}} - H_k\vec{x}_k^{\text{pre}}, \tag{11}$$

analogous to the standard Kalman filter, where the measurement is now replaced by the extrapolated measurement. If Eq. (9) is inserted, we finally obtain (6). Thus we showed, that the simple definition (6) for the measurement residuum is sufficient for delayed, linear filter problems. In Section 3, we demonstrate that this approach results in a navigation filter which is stable within a hardware-in-the-loop test with real, delayed sensor measurements.

In order to compute $\vec{x}(t)^{\text{est}}$, the values $\vec{x}_{s-1}^{\text{est}}, \vec{x}_s^{\text{est}}$ must be stored. If the measurement is delayed by a maximum of N samples, the last N estimates need to be stored for future use. Thus, by adapting the Kalman filter slightly using (6) and (8), we result in a simple filter technique for linear filter problems which can handle delayed measurements.

We now state how the above presented filter can be applied for rendezvous: the Hill equations (1) are discretized with respect to time by using the Euler method and are rewritten to the form (2a). Therefore, let $\vec{x}_k = (\vec{p}_k, \vec{v}_k) \in \mathbb{R}^6$ be the state vector and $\vec{u}_k = (1/m)\vec{f}_k$ the input vector. As above, the subscript k denotes that a function is evaluated at time t_k, e.g. $\vec{p}_k := \vec{p}(t_k)$.

The matrices F_k and G_k in the system model (2a) are set to

$$F_k = \mathrm{Id}_6 + \delta t_k \begin{pmatrix} 0 & 0 & 0 & 1 & 0 & 0\\ 0 & 0 & 0 & 0 & 1 & 0\\ 0 & 0 & 0 & 0 & 0 & 1\\ 0 & 0 & 0 & 0 & 0 & 2\omega_0\\ 0 & -\omega_0^2 & 0 & 0 & 0 & 0\\ 0 & 0 & 3\omega_0^2 & -2\omega_0 & 0 & 0 \end{pmatrix}, \tag{12}$$

$$G_k = \delta t_k \begin{pmatrix} 0 & 0 & 0\\ 0 & 0 & 0\\ 0 & 0 & 0\\ 1 & 0 & 0\\ 0 & 1 & 0\\ 0 & 0 & 1 \end{pmatrix}, \tag{13}$$

where Id_6 denotes the 6×6 identity matrix and $\delta t_k := t_{k+1} - t_k$. The output of the measurement system $\vec{z}_k$ is a measurement of the position $\vec{p}_k$. Therefore the matrix H_k in (2b) is set to

$$H_k = \begin{pmatrix} 1 & 0 & 0 & 0 & 0 & 0\\ 0 & 1 & 0 & 0 & 0 & 0\\ 0 & 0 & 1 & 0 & 0 & 0 \end{pmatrix}. \tag{14}$$

2.3.3. Guidance and control

The guidance system provides reference values and generates a position profile. The objective of guidance is to define and force a state that the spacecraft should finally reach. For VIBANASS, a guidance trajectory has been chosen which consists of (i) a hold point at an initial position, e.g. at 18 m distance, (ii) a smooth approach to 5 m with a maximum velocity of 5 cm/s, (iii) a second hold point at 5 m, (iv) a smooth approach to 1.8 m with a decreased velocity of 5 mm/s and (v) a final hold point at 1.8 m. At the intermediate hold point at 5 m distance to the target, a switch of the camera system from mono mid range to stereo close range camera takes place.

A PID controller compares the reference values provided by the guidance system with the actual values. The result of the navigation filter, the estimated position and velocity, serves as an input for the orbit controller. Let $e(t)$ be the position error, i.e. the difference between estimated

position and guidance value and $\dot{e}(t)$ the velocity error, i.e. the difference between estimated velocity and guidance velocity. The controller output $u(t)$ is a weighted sum of $e(t)$, its integral and the velocity error $\dot{e}(t)$:

$$u(t) = k_P\, e(t) + k_I \int_0^t e(\tau)\, \mathrm{d}\tau + k_D\, \dot{e}(t), \tag{15}$$

where k_P, k_I and k_D are called proportional gain, integral gain and derivative gain respectively.

By using the well-known PID control theory [29,26] an initial guess of these parameters has been calculated based on the desired damping behavior and negligence of cross couplings between the different components (see (1)). After system integration a final tuning has been performed by small adaptations of the control parameters.

The controller computes force commands for the thrusters. In the simulation, actuator systems cannot be represented by real-hardware and are consequently part of the numerical simulator. The simplified actuator system implemented for VIBANASS only limits the forces due to the specified maximum allowed thrust level.

3. Results

Several closed loop rendezvous tests were performed in the framework of the VIBANASS test campaign at the HiL simulator EPOS. Due to simple simulation architecture and simple interface structures we faced a time delay of 2–3 s (time-varying, about 0.5 s standard derivation). These delays are representative for delays occurring during teleoperation [3,7,8]. Hence, the behavior of the GNC system under delay conditions similar to a real, ground-based rendezvous could be tested.

3.1. Hold point at 5 m

The first test was a closed loop rendezvous simulation at a hold point at 5 m using the mono, mid range camera. The

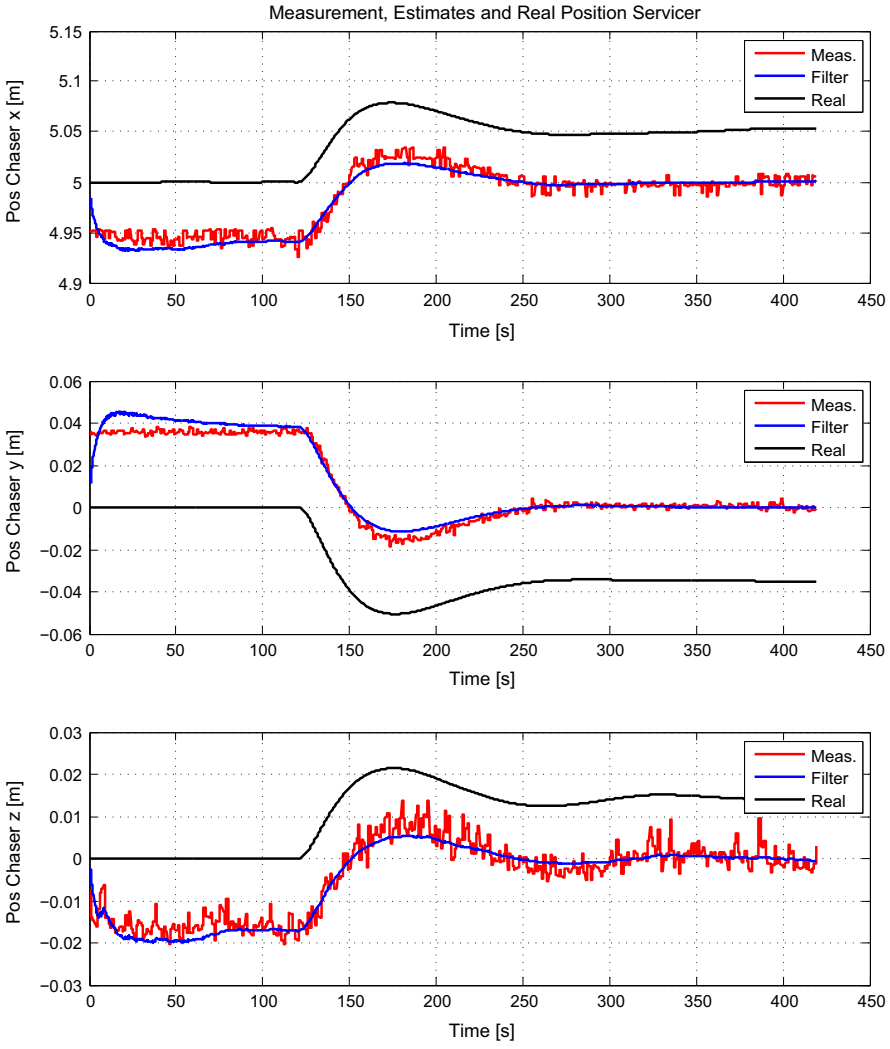

Fig. 6. Hold point at 5 m; absolute values: measurement, filter and real position.

image processing result served as an input for the navigation filter. Fig. 6 shows the measurement, filter estimate and real value for the three components of the position. The closed loop was started after 120 s, i.e. the first controller commands were computed based on the filter estimates after 120 s. The estimation error was approx. 5 cm in x-, approx. 3.8 cm in y- and approx. 1.5 cm in z-direction. After the closed loop was started, the filter estimates were fed back to the controller. As the guidance values were 5 m for x and 0 m for both y and z, the satellite in the simulation moved such that the filter estimates matched with the guidance values. Therefore, the systematic measurement errors (measurement biases) induced an error in the real position compared to the guidance values.

3.2. Approach with image processing

An approach from 18 m to approximately 2 m was performed using the image processing result as an input for the navigation system. The guidance trajectory was a continuous approach from 18 m to 1.8 m with a hold point at 5 m as described in Section 2.3.3.

Fig. 7 shows the measurement, the filter estimates and the real position of the chaser (x-component). The approach took place from the x-direction in the Clohessy Wiltshire frame (V-Bar), thus x corresponds to the distance between chaser and target.

Fig. 8 presents the error of the measurement and of the filter. The x-component (distance) was most difficult to measure from mono camera images. Therefore, the x-measurement was less accurate than the y- and z-measurement.

After approximately 80 s the loop was closed, i.e. the filter estimates were fed to the controller and the first controller commands were computed. Due to measurement errors which did not have zero mean, the controller used erroneous values for the actual position leading to performance errors, similar to described in Section 3.1. At 5 m (after ca. 900 s), the hold point was reached and a switch to stereo camera was accomplished. The measurement error was much smaller after the switchover to stereo camera, which resulted in a better performance. This can clearly be seen considering for example the y-coordinate in Fig. 8.

Fig. 9 shows the average measurement error with respect to the distance. At the start point at 18 m, there was a measurement error of 30–35 cm in the distance (cf. x-component). A smaller distance compared to the real distance was measured (negative error). Caused by the delay of the measurement, a positive distance error was noted for distances <14 m ($=$a too large distance measurement). At about 15 m the negative error of the measurements and the positive error induced by the delay canceled each other.

At approximately 10 m, there was a velocity of 5 cm/s, cf. panel 4 in Fig. 9 which shows the average velocity in the x-direction with respect to the distance. Having a time delay of 2–3 s, a distance error of 10–15 cm had been expected. This was consistent with the experimental results at 10 m, see panel 1 of Fig. 9. During the acceleration and deceleration phase, the error caused by the delay was smaller since the velocity was smaller. This resulted in a local maximum of the error in the x-coordinate at 10–11 m.

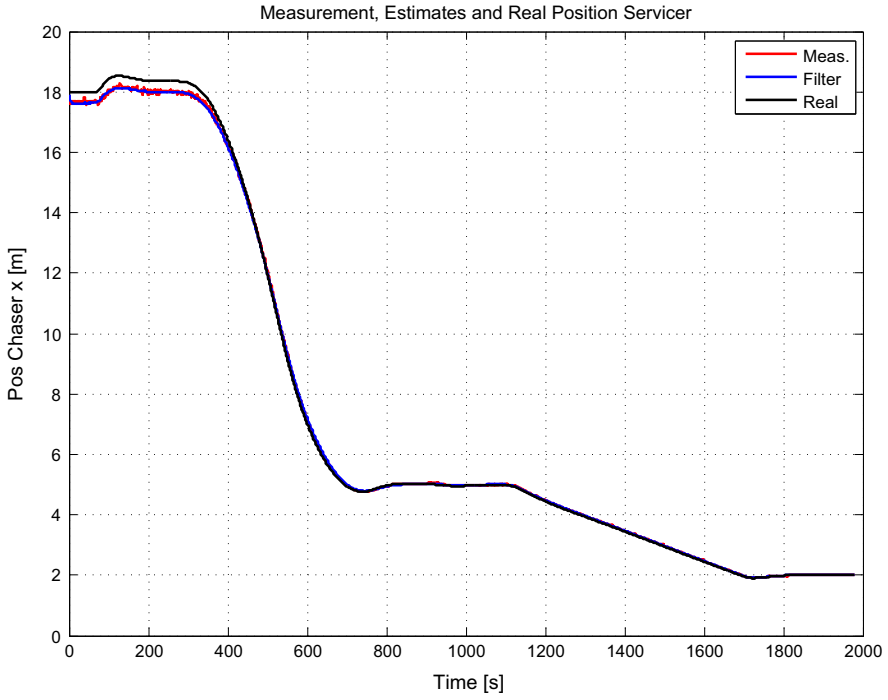

Fig. 7. Approach 18–2 m; absolute values of measurement, filter and real position, x-component. (For interpretation of the references to color in this figure caption, the reader is referred to the web version of this paper.)

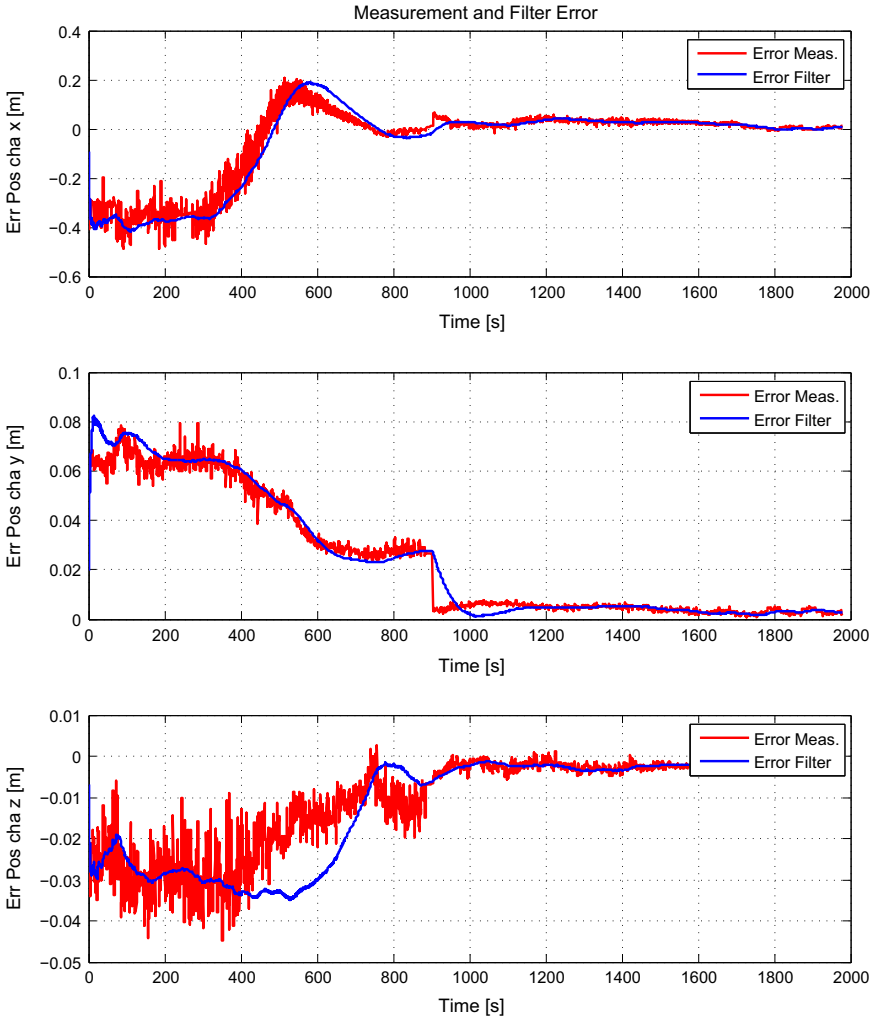

Fig. 8. Approach 18–2 m: measurement, filter error.

At distances between 14 m and 18 m, the pure measurement error dominated the delay error which resulted in a negative total distance error.

At the second hold point at 5 m, the measurement improved. The delay had smaller effect since the velocity was almost 0. When starting the second approach phase with the stereo camera, the error slightly increased as delays resulted in a positive error. However during the whole approach from 18 m to 2 m, a decrease of the absolute value of the error could be noted. With smaller distance to the target, the accuracy could be improved.

3.3. *Approach with operator in the loop*

An approach from 18 m to 2 m was performed with an operator in the loop. The same guidance trajectory as in Section 3.2 was used. The operator used a space mouse and marked the outer edges of the target body in the camera images during mid-range and the boundary of the nozzle during close range rendezvous, see Fig. 10. From the detected edges the relative position could be computed. The operator therefore replaced the first part of the image processing: the detection and localization of edges in the camera image.

Figs. 11–13 show the results of this test, in detail the absolute, filter and measured x-value, the error of filter estimates and measurements for all components and the measurement error depending on the distance. Measurement errors and little measurement rate caused the system to oscillate at the initial position at 18 m. But the amplitude of the oscillations was decreasing. Thus the system was still stable. When the distance became smaller during the approach, the measurements became more accurate. For distances <5 m, the measurement error decreased significantly due to the switch from mid range to close range camera.

4. Discussion

The results of the first test at 5 m hold point show the general behavior of the GNC system if the measurement

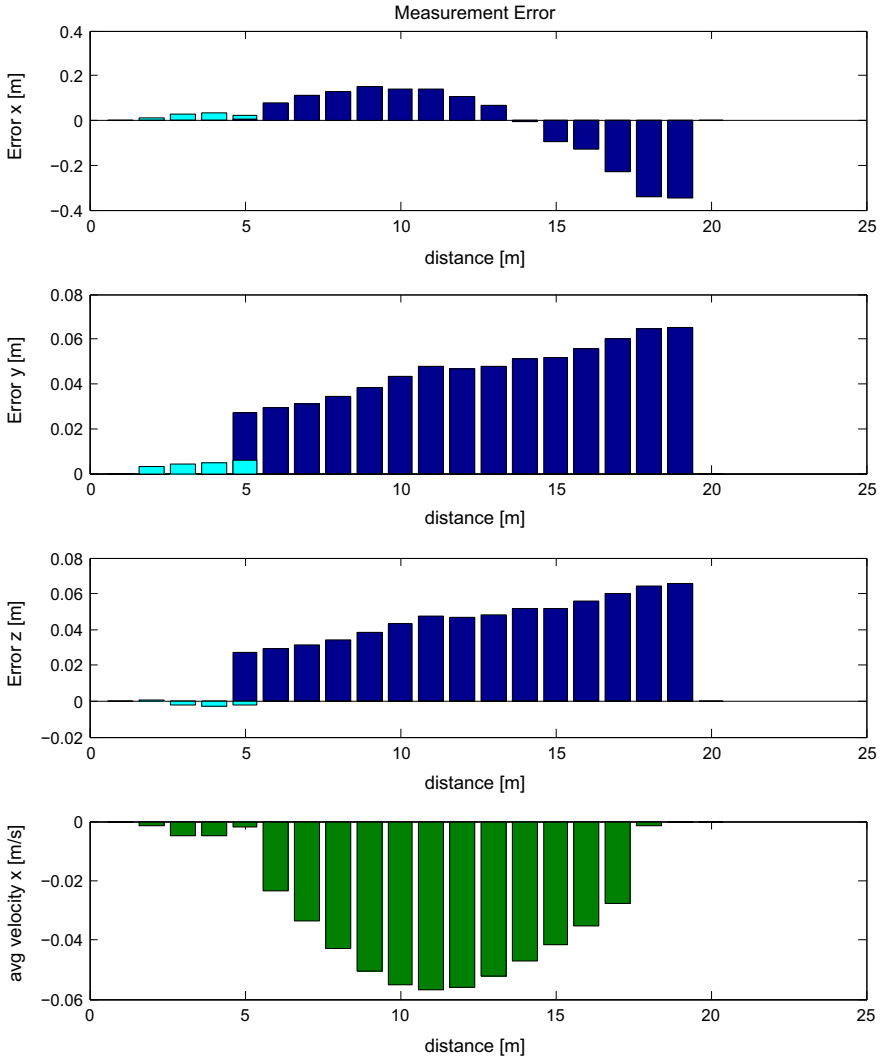

Fig. 9. Approach 18–2 m: panels 1–3: measurement error with respect to distance, blue: mid range, cyan: close range camera, panel 4: average velocity (x-component) w.r.t. distance. (For interpretation of the references to color in this figure caption, the reader is referred to the web version of this paper.)

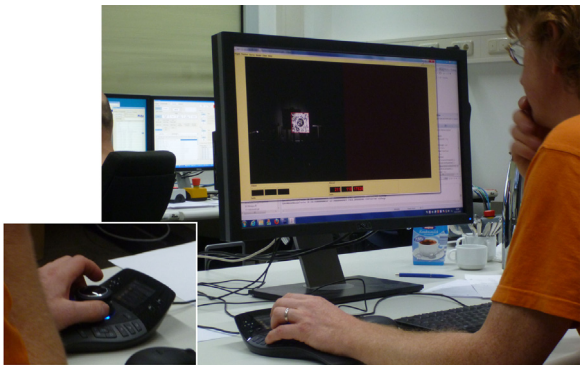

Fig. 10. Image processing operator during VIBANASS test campaign—manual detection of the client in camera images using a space mouse.

output has a systematic error. To transform measurements from a camera coordinate system to world coordinates a hand-eye calibration is needed [30]. Hand-eye calibration data was not available during the experiment. Therefore the main source of measurement errors is missing hand-eye calibration. These biases also affect the estimation error, since the filter can smooth the raw measurement data, but cannot correct biases.

The systematic measurement errors observed during the approach (recall e.g. Fig. 8) are again caused by missing calibration but also by the time delay. The delay mainly affects the distance component. Further, the accuracy of the measurements is limited by the resolution of the image: at large distances, changes in position of some centimeters cause only sub-pixel changes in the position of the target in the image. Therefore, these changes are hard to recognize by an image processing system.

The measurement error in x at zero average velocity (e.g. at hold points) decreases with decreasing distance. The measurement error induced by the time delay increases with increasing velocity. Although delayed measurements are extrapolated, recall Eq. (9), they can be a

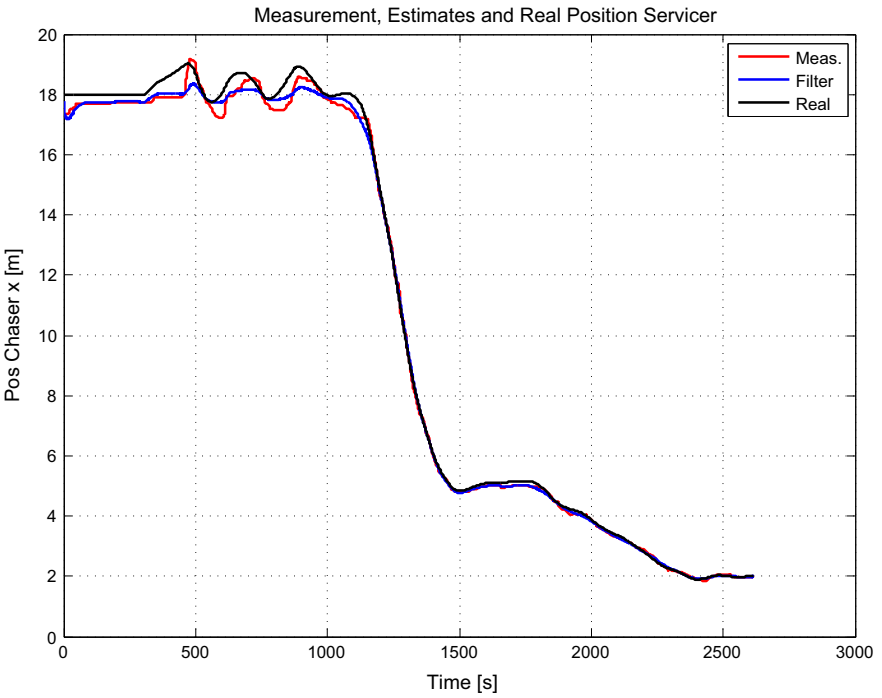

Fig. 11. Approach 18–2 m with operator in the loop; absolute values of measurement, filter and real position, *x*-component.

source of error since the extrapolation can also be erroneous. For example, if there are speed changes, the position profile will be non-linear and the linear extrapolation of the position measurement will be inaccurate. At all distances however, the error in x is $<2\%$ of the distance during the test where the image processing result was used as a measurement input for the navigation system.

In the y- and z-coordinate, the time delay has no noticeable effect as there is a constant guidance value in the y- and z-direction during the approach. The error decreases with decreasing distance to the target since the target becomes larger in the camera images. Image processing errors e.g. 1 pixel result in a smaller error of the final position measurement compared to larger distances. The error in y and z is about 0.5% of the distance when using the mid range camera. A small peak at 11 m (cf. Fig. 9) seems to be a single effect and could be caused by problems in tracking the outer edges of the target. Maybe there was some edge in the background of the EPOS laboratory near the target edges which can cause problems in image processing and tracking.

After the switchover to the stereo camera, the error significantly improves. At a close range, the error in the y- and z-component is approximately 0.1–0.2% of the distance.

Compared to the test with image processing, the approach with an operator in the loop was accomplished under more difficult conditions:

- less accurate measurements: the target is hard to track accurately by the operator, in particular at large distances,
- reduced measurement rate: 0.2–0.3 Hz average rate, compared to the image processing rate of 1 Hz,
- less continuous measurements, big deviation in the time between two measurements (sometimes 2–3 s, sometimes 10 s difference between two measurements),
- positive and negative measurement errors alternate.

Despite these conditions, a stable approach could be accomplished. The errors and the oscillations were naturally higher compared to the tests with image processing.

The main goal of the closed loop rendezvous simulation was to perform a safe approach from about 18 m to a point prior to docking. The closed loop proved to be stable. Small systematic measurement errors and varying time delays which are expected to occur during ground-based on-orbit servicing missions could be handled. Those affected the accuracy and the performance of the entire system but the control loop kept stable. Since time delay is a critical issue for the stability of a control loop, it is useful to work on methods that compensate for time delay. If the approach velocities are small and the delay time in the range of some seconds, time delays can be handled during rendezvous if the GNC system is accordingly adapted for delayed measurements.

In the work of Bell et al. [17], time delays of 2.8 s are observed during hardware-in-the-loops tests with a 3D LIDAR. The delay can be partly compensated by a Kalman filter which uses a guess of 2.0 s of time delay. The time difference of 2.8 s is measured after the experiments. It is not described if and how the standard Extended Kalman filter is adapted for time delays. In our experimental setup,

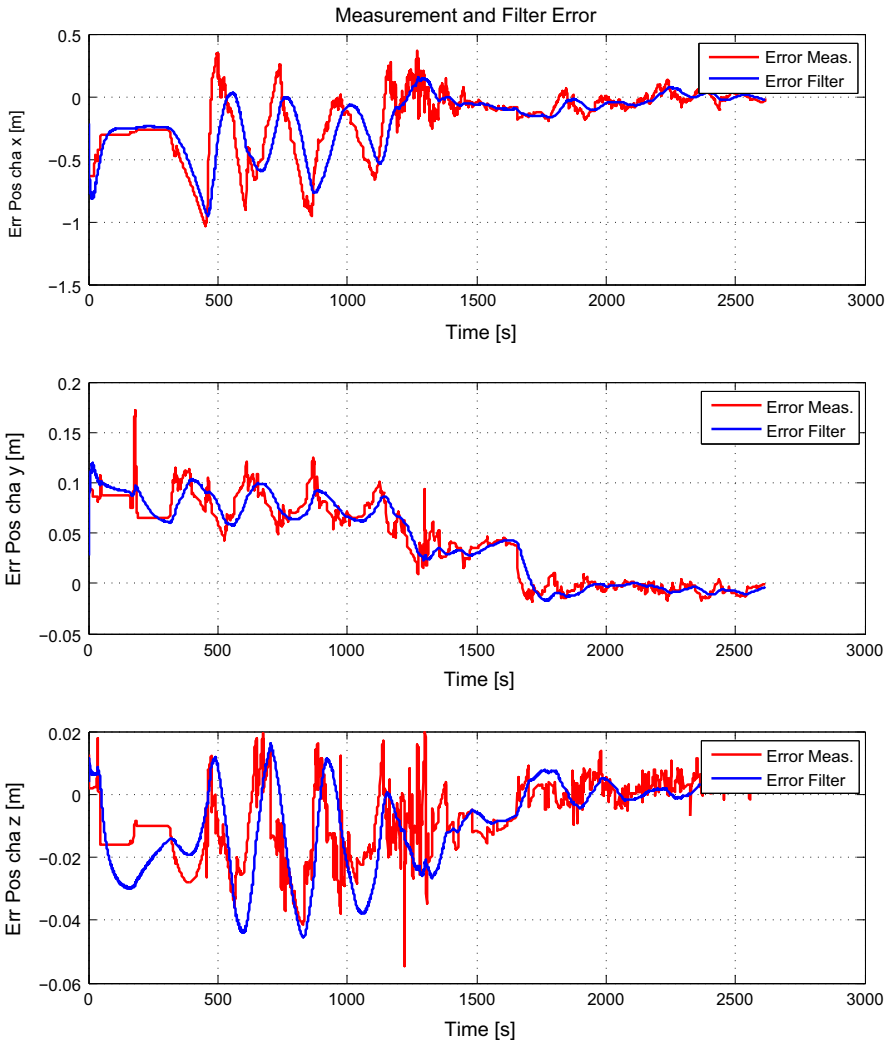

Fig. 12. Approach 18–2 m with operator in the loop: measurement, filter error.

we are able to measure the time of the image capturing using a GPS receiver. Further, we adapted the Kalman filter slightly to handle time delays. For that we store not only the actual filter estimate but a certain number of previous estimates which are necessary to compute an estimate of the state at the time of the image capturing, recall (7). In addition, there is no restriction on the time delays in our setup. The delay can be time-varying (i.e. non-constant) and need not be a multiple of the sample time of the filter.

In summary, on-orbit servicing with telepresence is an alternative to autonomous servicing, where the GNC system is executed on the servicer's on-board computer without or with limited operator intervention. The telepresence servicing method seems to be a promising option when the GNC system is adapted for time delays.

5. Conclusion

We presented a concept for closed loop rendezvous simulation involving optical sensors. The GNC system could cope with delayed measurements and enabled a stable approach. Similar time delays are expected for future servicing missions with telepresence, where the data processing and GNC algorithms will be computed on ground. During the VIBANASS test campaign at EPOS 2.0, a camera system and the developed GNC system were embedded into a rendezvous simulation and tested in a closed loop mode. Safe and stable approaches from 18 m to 2 m with two camera systems (mono for mid range, stereo for close range) were performed. The concept was able to use both image processing results and measurements by an operator. However, the image processing yielded more accurate measurements and resulted in a better overall performance of the GNC system.

Acknowledgment

The authors would like to thank Peter Rank, Quirin Mühlbauer and Sven Semler from Kayser-Threde GmbH and Jorg Vogel from DLR's Institute of Robotics and Mechatronics for the pleasant and successful cooperation during the VIBANASS test campaign at EPOS.

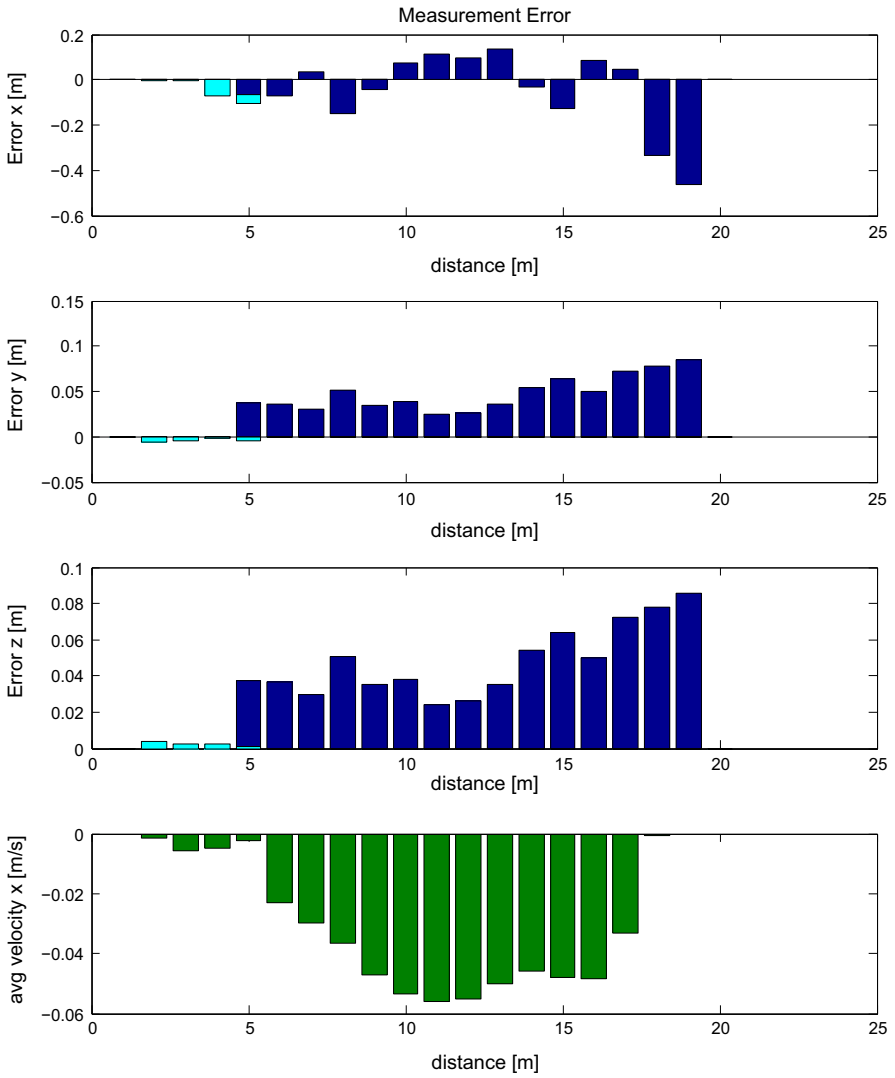

Fig. 13. Approach 18–2 m with operator in the loop: panels 1–3: measurement error with respect to distance, blue: mid range, cyan: close range camera, panel 4: average velocity (*x*-component) w.r.t. distance. (For interpretation of the references to color in this figure caption, the reader is referred to the web version of this paper.)

References

[1] A. Ellery, J. Kreisel, B. Sommer, The case for robotic on-orbit servicing of spacecraft: spacecraft reliability is a myth, Acta Astronaut. 63 (2008) 632–648.

[2] E. Stoll, J. Letschnik, U. Walter, J. Artigas, P. Kremer, C. Preusche, G. Hirzinger, On-orbit servicing, IEEE Robot. Autom. Mag. 16 (2009) 29–33.

[3] F. Sellmaier, T. Boge, J. Spurmann, S. Gully, T. Rupp, F. Huber, On-orbit servicing missions: challenges and solutions for spacecraft operations, in: Proceedings of AIAA SpaceOps, Huntsville, Alabama, 2010.

[4] T. Wolf, D. Reintsema, B. Sommer, Mission DEOS—proofing the capabilities of German's space robotic technologies, in: Proceedings of International Symposium on Artificial Intelligence, Robotics and Automation in Space (i-SAIRAS), European Space Agency, Turin, Italy, 2012.

[5] S.-I. Nishida, S. Kawamoto, Y. Okawa, F. Terui, S. Kitamura, Space debris removal system using a small satellite, Acta Astronaut. 65 (2009) 95–102.

[6] K. Landzettel, C. Preusche, A. Albu-Schäffer, D. Reintsema, B. Rebele, G. Hirzinger, Robotic on-orbit servicing—DLR's experience and perspective, in: Proceedings of International Conference on Intelligent Robots and Systems, Beijing, China, 2006, pp. 4587–4594.

[7] L. Tarabini, J. Gil, F. Gandia, M.A. Molina, J.M. Del Cura, G. Ortega, Ground guided CX-OLEV rendezvous with uncooperative geostationary satellite, Acta Astronaut. 61 (2007) 312–325.

[8] T. Imaida, Y. Yokokohji, T. Doi, M. Oda, T. Yoshikawa, Ground-space bilateral teleoperation of ETS-VII robot arm by direct bilateral coupling under 7-s time delay condition, IEEE Transactions on Robotics and Automation 20 (3) (2004) 499–511.

[9] O. Ma, A. Flores-Abad, T. Boge, Use of industrial robots for hardware-in-the-loop simulation, Acta Astronaut. 81 (2012) 335–347.

[10] T. Boge, H. Benninghoff, M. Zebenay, F. Rems, Using robots for advanced rendezvous and docking simulation, in: Proceedings of Simulation and EGSE Facilities for Space Programmes (SESP), Noordwijk, The Netherlands, 2012.

[11] H. Benninghoff, T. Boge, T. Tzschichholz, Hardware-in-the-loop rendezvous simulation involving an autonomous guidance, navigation and control system, Adv. Astronaut. Sci. 145 (2012) 953–972.

[12] W. Xu, B. Liang, C. Li, Y. Xu, Autonomous rendezvous and robotic capturing of non-cooperative target in space, Robotica 28 (2010) 705–718.

[13] B. Qiao, S. Tang, K. Ma, Z. Liu, Relative pose and attitude estimation of spacecrafts based on dual quaternion for rendezvous and docking, Acta Astronaut. 91 (2013) 237–244.
[14] J. Sommer, I. Ahrns, GNC for rendezvous in space with an uncooperative target, in: Proceedings of 5th International Conference on Spacecraft Formation Flying Missions and Technologies, Munich, Germany, 2013.
[15] S. D'Amico, J.-S. Ardaens, G. Gaias, H. Benninghoff, B. Schlepp, J.L. Jørgensen, Noncooperative rendezvous using angles-only optical navigation: system design and flight results, J. Guid. Control Dyn. 36 (2013) 1576–1595.
[16] G. Guglieri, F. Maroglio, P. Pellegrino, L. Torre, A ground facility to test GNC algorithms and sensors for autonomous rendezvous and docking, Adv. Astronaut. Sci. 145 (2012) 933–952.
[17] R. Bell, T. Morphopoulos, J. Pollack, J. Collins, J.R. Wertz, R.E. Van Allen, Hardware-in-the-loop tests of an autonomous GN&C system for on-orbit servicing, in: Proceedings of AIAA-LA Section/SSTC Responsive SpaceConference, 2003.
[18] T. Boge, T. Wimmer, O. Ma, M. Zebenay, EPOS—a robotics-based hardware-in-the-loop simulator for simulating satellite RvD operations, in: Proceedings of International Symposium on Artificial Intelligence, Robotics and Automation in Space (i-SAIRAS), Sapporo, Japan, 2010.
[19] C. Kaiser, P. Rank, K. Landzettel, T. Boge, M. Turk, Vision based navigation for future on-orbit servicing missions, in: Proceedings of 62nd International Astronautical Congress (IAC), International Astronautical Federation, 2011.
[20] T. Wimmer, T. Boge, Q. Mühlbauer, EPOS: a hardware-in-the-loop robotic simulation assembly for testing automated rendezvous and docking GNC sensor payloads, in: Proceedings of 8th International ESA Conference on Guidance, Navigation and Control Systems (GNC), European Space Agency, Karlovy Vary, Czech Republic, 2011.
[21] Q. Mühlbauer, L. Richter, C. Kaiser, P. Hofmann, Robotics space systems and subsystems for advanced future programmes, in: Proceedings of International Symposium on Artificial Intelligence, Robotics and Automation in Space (i-SAIRAS), European Space Agency, Turin, Italy, 2012.
[22] W. Xu, B. Liang, Y. Xu, Survey of modeling, planning, and ground verification of space robotic systems, Acta Astronaut. 68 (2011) 1629–1649.
[23] Q. Mühlbauer, P. Rank, C. Kaiser, On-ground verification of VIBANASS (vision based navigation sensor system): capabilities and results, in: Procedings of 12th Symposium on Advanced Space Technologies in Robotics and Automation, Noordwijk, The Netherlands, 2013.
[24] N. W. Oumer, G. Panin, 3D point tracking and pose estimation of a space object using stereo images, in: Proceedings of 21st International Conference on Pattern Recognition (ICPR), International Association of Pattern Recognition, Tsukuba, Japan, 2012.
[25] J.R. Wertz, Attitude Determination and Control, Kluwer Academic Publishers, Dordrecht, Boston, London, 2002.
[26] W. Fehse, Automated Rendezvous and Docking of Spacecraft, Cambridge Aerospace Series, Washington, D.C., 2003.
[27] R.E. Kalman, A new approach to linear filtering and prediction problems, Trans. ASME, J. Basic Eng. 83 (1960) 35–45.
[28] P. Zarchan, H. Musoff, Fundamentals of Kalman Filtering: A Practical Approach, vol. 190, Progress in Astronautics and Aeronautics, Cambridge, Massachusetts, 2000.
[29] J. Lunze, Regelungstechnik 1, Systemtheoretische Grundlagen, Analyse und Entwurf einschleifiger Regelungen, Springer, Berlin, Heidelberg, 2001.
[30] K. Strobl, G. Hirzinger, Optimal hand-eye calibration, in: Proceedings of International Conference on Intelligent Robots and Systems, Beijing, China, 2006.

Heike Benninghoff is a research associate in the On-Orbit Servicing team at DLR-GSOC in Oberpfaffenhofen, Germany. She received her diploma degree in mathematics in 2010 from the University of Regensburg. Her research interests comprise visual navigation, image processing, numerical analysis and HiL simulation.

Florian Rems got his diploma in aerospace engineering from the Technical University of Munich (TUM) in 2012. He is a research associate in the On-Orbit-Servicing group at the German Space Operations Center (GSOC). His work focuses on LIDAR technology for autonomous rendezvous navigation and on RvD simulation.

Toralf Boge received his Ph.D. in electrical engineering from Technical University Dresden in 2003. Since 2000 he works for DLR at GSOC. He is a team leader of On-Orbit Servicing team at GSOC. His areas of interest are sensors and GNC system for rendezvous and docking and HiL simulation.